

On the Rayleigh–Taylor Instability of Radio Bubbles in Galaxy Clusters

Fabio Pizzolato¹ * and Noam Soker¹

¹*Department of Physics, Technion–Israel Institute of Technology, Haifa 32000 Israel*

30th July 2019

ABSTRACT

We consider the Rayleigh–Taylor instability in the early evolution of the rarefied radio bubbles (cavities) observed in many cooling–flow clusters of galaxies. The top of a bubble becomes prone to the Rayleigh–Taylor instability as the bubble rises through the intra–cluster medium (ICM). We show that while the jet is powering the inflation, the deceleration of the bubble–ICM interface is able to reverse the Rayleigh–Taylor instability criterion. In addition, the inflation introduces a drag effect which increases substantially the instability growth time. The combined action of these two effects considerably delays the onset of the instability. Later on, when the magnitude of the deceleration drops or the jet fades, the Rayleigh–Taylor and the Kelvin–Helmholtz instabilities set in and eventually disrupt the bubble. We conclude that the initial deceleration and drag, albeit unable to prevent the disruption of a bubble, may significantly lengthen its lifetime, removing the need to invoke stabilising magnetic fields.

Key words:

instabilities — methods: analytical — galaxies: clusters: cooling flows — galaxies: clusters: individual (A 2052) — galaxies: intergalactic medium — X-rays: galaxies: clusters

1 INTRODUCTION

The recent high spatial–resolution observations show that many clusters and groups of galaxies harbour bubbles (cavities) devoid of X–ray emission. Examples include Perseus (Fabian et al. 2000), Hydra A (McNamara et al. 2000), Abell 2052 (Blanton et al. 2001), Abell 2597 (McNamara et al. 2001), MKW 3s (Mazzotta et al. 2002), HCG 62 (Vrtilek et al. 2002), Abell 4059 (Heinz et al. 2002) Abell 478 (Sun et al. 2003), and MS 0735.6+7421 (McNamara et al. 2005); see also Bîrzan et al. (2004) for a systematic study. These bubbles are very low density regions inflated by the jets launched by the active galactic nuclei (AGN) sitting at the centres of these clusters. The lack of strong shocks at the rims of these bubbles shows that their inflation is quite gentle, and the bubbles are in approximate pressure equilibrium with the surrounding environment. On account of their lower density with respect to the outer environment, the bubbles rise buoyantly and sweep up some of the intra–cluster medium (ICM), as evident by the enhanced emission at their rims.

It would seem that the top of these bubbles is prone to the Rayleigh–Taylor Instability (hereafter, RTI). Indeed, the gravitational acceleration of the cluster pushes downwards, and the dense swept-up gas shell lies on the top of the thinner one inside the bubble itself. This RTI would be able to tear the bubble apart in few characteristic e–folding times

$$t_{\text{RT}} = \left(\frac{\lambda_h}{2\pi|g|} \right)^{1/2} = 2.2 \times 10^6 \text{ yr} \left(\frac{\lambda_h}{\text{kpc}} \right)^{1/2} \left(\frac{|g|}{10^{-7} \text{ cm s}^{-2}} \right)^{-1/2}, \quad (1)$$

where $|g|$ the modulus of the cluster gravitational acceleration and λ_h is the wavelength of the RT perturbation. The characteristic time (1) is about one order of magnitude less than the estimated ages of most bubbles (Bîrzan et al. 2004). This observation has prompted many authors (e.g. Brüggen and Kaiser 2001; Kaiser et al. 2005; Reynolds et al. 2005; Jones and

* E-mail fabio@physics.technion.ac.il

De Young 2005) to invoke an ordered magnetic field at the edge of the bubble to stabilise the bubble against the RTI. This scenario, however, may lead to some difficulties: if the magnetic field is ordered on a scale of the same order as the size of the bubble, its effect should be highly non-isotropic: it should be able to suppress very efficiently the RTI modes along the magnetic field lines, but not perpendicular to them. This is because the magnetic field cannot exert stress countering the instability a direction perpendicular to the field lines. If the field is tangled on scales much smaller than the bubble size, then it will have no effect on the large-wavelength modes which are those that tear the bubble apart.

In this paper we argue that a magnetic field is actually not necessary to explain the long lives of the radio bubbles. Extending the work by Soker et al. (2002) we shall show that during the first stages of its inflation a bubble is stable. In the early phase the inflation of the bubble is powered by a jet launched by the central AGN. While the jet is active the bubble radius grows with time as $R_b(t) \propto t^{3/5}$, implying that the acceleration \ddot{R}_b is *negative*. On the top of the bubble, then, this deceleration overcomes gravity, and the configuration of the bubble is RT-stable. Besides, the inflation introduces a drag effect which greatly reduces the instabilities growth rate. Only later, when $|\ddot{R}_b|$ decreases and the gravitational acceleration prevails, or the jet fades, does the instability set in, tearing the bubble apart. We show that the delay of the RTI onset is more than enough to explain the survival of old bubbles.

This paper is laid out as follows; in § 2 we discuss the properties of the bubbles, and sketch the physics developed in this paper. In § 3 we derive the equations of the RTI in a bubble actively inflated by a jet. In § 4 these equations are solved numerically, and the results are discussed in § 5. The last stage of the life of a bubble, after the extinction of the jet, is addressed in § 6. We summarise in § 7. Readers not interested in the mathematical details may harmlessly skip § 3 and § 4, jumping directly from § 2 to § 5.

2 THE RAYLEIGH–TAYLOR INSTABILITY IN BUBBLES

In this Section we refine the treatment by Soker et al. (2002) of the RTI of a bubble inflated by an AGN jet. The jet stops at a distance r_c from the cluster core, and hence it becomes the expansion centre of the bubble. The injected jet’s material passes through a strong shock and forms a very hot bubble, which later on keeps in approximate pressure equilibrium with its surroundings. On account of its low density, the bubble rises buoyantly into the ICM; during this process the expanding bubble sweeps up the ICM to form a thick shell of denser gas ahead of itself, as evident from the local enhanced X-ray luminosity. The X-ray observations also show a lack of strong shocks ahead of the bubble, so the swept-up shell and the gas inside the bubble move about with the same velocity. Because the shell density ρ_s is much higher than the density ρ_b inside the bubble, and since the gravitational acceleration is directed downward, the flow at the bubble’s top would be RT unstable if only gravity is considered. This simple picture, however, overlooks the bubble’s inflation process. We therefore consider a local frame of reference attached to a point P on the surface of the expanding bubble, and moving with it. A test particle in the non-inertial frame attached to P feels the radial (i.e., normal to the bubble’s surface) acceleration

$$\tilde{g} = -|g| \cos \theta - \ddot{R}_b(t), \quad (2)$$

where g is the cluster’s gravitational acceleration, θ the angle between the orthogonal to the bubble surface in P and the radial direction of the cluster, and $R_b(t)$ is the bubble radius at the instant t . If the jet supplies energy at the constant rate of \dot{E} , then

$$R_b(t) = \alpha \left(\dot{E} t^3 / \rho_a \right)^{1/5} \quad (3)$$

(Castor et al. 1975; Dokuchaev 2002), where ρ_a is the density of the ambient ICM. The dimensionless parameter α depends on the equation of state (EOS) of the gas inside the bubble: for a non-relativistic EOS $\alpha = 0.929$, while for a relativistic EOS $\alpha = 0.793$ (Dokuchaev 2002). For bubbles in cooling flow clusters the EOS is most likely to be somewhere in between these two extremes. It is worth noticing that Equation (3) assumes a uniform ambient density, which is not true for the stratified atmosphere of a cluster the bubble is embedded in. Nevertheless, in the following we shall adopt Equation (3) since it is but a secondary source of error. Moreover, if the cluster’s negative density gradient is considered, then the bubble’s top has the largest acceleration, making it more stable. Since the bubble’s top front is the least stable region, considering the density gradient will make the stabilising effect studied here more favourable.

The normal acceleration of a test particle residing on the bubble-ICM boundary in the non-inertial frame is therefore

$$\tilde{g} = -|g| \cos \theta + \frac{6}{25} \frac{R_b(t)}{t^2}. \quad (4)$$

Near the bottom of the bubble $\theta \sim \pi$, so \tilde{g} is always positive, meaning that the cluster’s gravitational acceleration and \ddot{R}_b have the same direction, and the total acceleration pulls towards the cluster centre. In this segment, the bubble is RT stable, because the lighter plasma (inside the bubble) lies above the denser one. Near the top of the bubble ($\theta \sim 0$) the acceleration (4) may be either positive or negative. At early stages (t small), \ddot{R}_b is large enough to overcome gravity, thus making \tilde{g} positive. The acceleration pulls upwards, and on account of the density stratification even this segment is RT-stable, without the need

of any magnetic field (as pointed out by Soker et al. 2002). On top of this, as discussed in § 3, the inflation introduces a drag effect on the perturbation, akin to the Hubble drag affecting the perturbations growth in an expanding Universe. Both in the cosmological context and here, this drag reduces the perturbations growth rate, further delaying the RTI onset. Later on, however the gravitational pull will prevail, and the RTI commence. The delay introduced by the early contribution of \dot{R}_b and by the drag term is more than enough to lengthen the life time of the bubble to a significant amount. The mathematical details justifying this statement are worked out in the following Section. Readers not particularly eager to afford them may skip § 3 and § 4 and go directly to Section 5.

3 RAYLEIGH–TAYLOR INSTABILITY OF AN EXPANDING BUBBLE

In this Section we derive the equations for the Rayleigh–Taylor instability of an expanding bubble. As customary in any perturbation analysis, it is convenient to decouple the “background” motion of the bubble (i.e., its expansion and uprising) from the motion associated to the true instability. To this aim we introduce a frame of reference moving with the expanding bubble. We consider an inertial frame of reference K , the origin of which coincides with the cluster’s centre. In this frame of reference the bubble’s centre O has coordinate $\mathbf{r}_b(t)$. We define a second frame K'' with its axes parallel to those of K , and centred on \mathbf{r}_b . Finally, we define the non-inertial frame K' with the same centre as K'' , which co-moves with the expanding bubble: in other words, the coordinates of any point expanding with the bubble are constant in the frame K' . The relation between the coordinates \mathbf{x}'' and \mathbf{r}' , referred to the frames K'' and K' respectively, is

$$\mathbf{x}'' = a(t) \mathbf{r}', \quad (5)$$

where (from Equation (3)) we define the expansion scale factor

$$a(t) = R_b(t)/R_b(t_0) = (t/t_0)^{3/5}, \quad (6)$$

where t_0 is an arbitrary reference time. Putting together all the previous equations, the relation between the inertial frame K and the co-moving frame K' is

$$\mathbf{x} = \mathbf{r}_b(t) + a(t) \mathbf{r}'. \quad (7)$$

This formula allows us to write down a set of hydrodynamic equations in the co-moving frame K' . The advantage of this approach is that the unperturbed equations in K' are time-independent, allowing a more direct approach to the subsequent perturbation analysis.

We write the usual gas dynamic equations in the inertial frame K (e.g. Landau and Lifshits 1987)

$$\frac{\partial \rho}{\partial t} + \nabla \cdot (\rho \mathbf{v}) = 0 \quad (8a)$$

$$\rho \frac{d\mathbf{v}}{dt} + \nabla P - \rho \mathbf{g} = 0. \quad (8b)$$

From the coordinate transformation (7) and the equality $t = t'$ (K and K' have the same time units), we retrieve the relations between the derivatives in K and K' :

$$\frac{\partial}{\partial t} = \frac{\partial}{\partial t'} - \frac{\mathbf{v}_b + \dot{a} \mathbf{r}'}{a} \cdot \nabla' \quad (9a)$$

$$\nabla = \frac{1}{a} \nabla'. \quad (9b)$$

In the first equality we assume that during the relevant evolutionary phases for our study the buoyancy velocity $\mathbf{v}_b = \dot{\mathbf{r}}_b$ is negligible in comparison to the expansion velocity $\dot{a} \mathbf{r}'$. Plugging these into Equations (8), after some algebra, we get the following set of equations in the co-moving frame K' :

$$\frac{\partial \rho'}{\partial t'} + \nabla' \cdot (\rho' \mathbf{v}') = 0 \quad (10a)$$

$$\rho' \left(\frac{d' \mathbf{v}'}{dt'} + \frac{\ddot{a}}{a} \mathbf{r}' + 2 \frac{\dot{a}}{a} \mathbf{v}' \right) + \frac{1}{a} \left(\nabla' P' - \rho' \mathbf{g} \right) = 0, \quad (10b)$$

where we have introduced the new co-moving variables

$$\rho' = \rho a^3 \quad (11a)$$

$$\mathbf{v}' = \frac{\mathbf{v} - \dot{a} \mathbf{x}'}{a} \quad (11b)$$

$$P' = P a^2, \quad (11c)$$

and $d'/dt' = \partial_{t'} + \mathbf{v}' \cdot \nabla'$ is the convective derivative in the co-moving frame.

3.1 The Unperturbed Configuration

As noted in the discussion following Equation (4), the most prone segment to the RTI is the top of the bubble. Where necessary, therefore, we shall limit our analysis to this portion of the bubble. Before studying the perturbations, it is necessary to define a “background” unperturbed configuration. In the present case it is, obviously, the configuration of an expanding bubble. This is described by the set of equations (10) with $\mathbf{v}' = 0$. The co-moving continuity equation (10a) yields $\partial_{t'}\rho' = 0$, i.e. ρ' is constant with time; the density ρ in the inertial frame is $\rho \propto a^{-3}$, i.e. the mass contained within any given volume expanding with the bubble is constant, as expected.

As our X-ray observations show, there is no signature of strong shocks between the bubble interior and the overlying swept-up shell. For this reason, we assume that the shell and the adjacent segment of the bubble interior move with the same speed, and the only difference between them is in density. We denote with R the co-moving coordinate of the interface between the thick shell and the bubble interior. The unperturbed density profile undergoes a sharp discontinuity across the edge of the bubble, passing from the low value ρ_b inside the bubble ($r' < R$) to the ambient value ρ_a outside it ($r' > R$). We put $\rho_s \sim \rho_a$, i.e. we neglect the density enhancement ahead of the bubble due to the swept-up material, since its effect is small. Our unperturbed co-moving density profile is then

$$\rho' = \begin{cases} \rho_a & r' > R \\ \rho_b & r' < R. \end{cases} \quad (12)$$

The co-moving unperturbed static Euler equation

$$\nabla' P' = \rho' (\mathbf{g} - \ddot{\mathbf{a}} \mathbf{r}'), \quad (13)$$

can be projected in the radial and tangent direction with respect to the co-moving frame K' :

$$\frac{\partial P'}{\partial r'} = \rho' (g_{r'} - \ddot{a} r'), \quad (14)$$

$$\nabla_h P' = \rho' g_h, \quad (15)$$

where $g_{r'}$ and g_h are respectively the projections of the cluster gravitational acceleration parallel and perpendicular to the direction of the bubble’s radius. It is quite apparent that the term g_h is non-zero if the point P is not aligned with the line joining the bubble and the cluster centres. On the top of the bubble, which concerns us most, $g_h \sim 0$, so $\nabla_h P \sim 0$, and the pressure gradient is purely radial. Here, Equation (14) defines a local hydrostatic equilibrium in the effective gravity

$$g_{r'} - \ddot{a} r' = -[|g| + \ddot{a}(t) r'] = -\tilde{g}. \quad (16)$$

The overall effective gravity is *smaller* than expected from the cluster’s contribution alone, since $\ddot{a}(t) < 0$.

3.2 Lagrangian Perturbation Analysis

Having determined the properties of the equilibrium solution, we pass to study the perturbation to the inflating bubble. For the sake of simplicity, from now on we omit all the primes referred to the co-moving frame K' . It should be clear, however, that all the variables hereafter refer to that frame.

The perturbation analysis is most easily performed in the Lagrangian formalism (see e.g. Shapiro and Teukolsky 1983 for a nice introduction). Let $\boldsymbol{\xi}(\mathbf{x}, t)$ be the displacement of a fluid element due to the perturbation. The Lagrangian density perturbation $\Delta\rho$, i.e. the perturbation measured in a frame of reference moving with the unperturbed flow, is

$$\Delta\rho = -\rho \nabla \cdot \boldsymbol{\xi}. \quad (17)$$

In the context of the study of the RTI, it is customary to assume that the perturbation is incompressible. This assumption holds if the RTI growth time (Equation (1)) is shorter than the time

$$t_{\text{sound}} \sim \lambda/c_s \sim 1.0 \times 10^6 \text{ yr} \left(\frac{\lambda_h}{\text{kpc}} \right) \left(\frac{T}{10 \text{ keV}} \right)^{-1/2}. \quad (18)$$

taken by a sound wave to cross the perturbation itself. The rationale of this request is that if t_{sound} is very short, then the sound waves are very effective in keeping the pressure equilibrium within the portions of the perturbation. In our case the incompressibility requirement $t_{\text{RT}} \ll t_{\text{sound}}$ does not seem to hold. However, the compressibility affects little the growth rate of the RT perturbation when the density ratio ρ_a/ρ_b is large, as occurs in the present case (see e.g. Baker 1983; Livescu 2004). Therefore, it is safe to adopt the incompressibility assumption $\Delta\rho = 0$: from Equation (17), this is equivalent to

$$\nabla \cdot \boldsymbol{\xi} = 0. \quad (19)$$

The a -th component of the perturbed Euler equation reads

$$\rho \left[\frac{d^2 \xi_a}{dt^2} + 2 \frac{\dot{a}}{a} \frac{d\xi_a}{dt} \right] + \nabla_a (\Delta P) - (\nabla_s P_0) \nabla_a \xi_s = 0, \quad (20)$$

where the pressure gradient may be expressed in terms of the unperturbed Euler equation $\nabla P = \rho \tilde{\mathbf{g}}$. It is convenient to decompose the displacement vector $\boldsymbol{\xi}$ to a radial component ξ and a tangential (or horizontal) component $\boldsymbol{\xi}_h$:

$$\boldsymbol{\xi} = \begin{bmatrix} \xi \\ \boldsymbol{\xi}_h \end{bmatrix}. \quad (21)$$

The condition of incompressibility (19) then reads

$$\frac{1}{r^2} \frac{\partial}{\partial r} (r^2 \xi) + \nabla_h \cdot \boldsymbol{\xi}_h = 0. \quad (22)$$

If we may neglect the radius of curvature of the bubble, this simplifies to

$$\frac{\partial \xi}{\partial r} + \nabla_h \cdot \boldsymbol{\xi}_h \sim 0. \quad (23)$$

This approximation is permitted so long as the size λ of a perturbation (which is stretched by the bubble inflation itself) is much smaller than bubble radius R_b . Although we are also interested in perturbation with $\lambda \sim R_b$, we will use this approximation throughout the rest of the paper, as it is adequate enough for our goal of showing that no stabilising magnetic fields are needed to explain the survival of old bubbles.

We take advantage of the fact that the unperturbed quantities only depend on the radial coordinate r to separate out the dependence on the horizontal coordinates:

$$\xi = \xi(r, t) e^{i\mathbf{k}_h \cdot \mathbf{x}} \quad (24a)$$

$$\boldsymbol{\xi}_h = \boldsymbol{\xi}_h(r, t) e^{i\mathbf{k}_h \cdot \mathbf{x}} \quad (24b)$$

$$\Delta P = \Delta P(r, t) e^{i\mathbf{k}_h \cdot \mathbf{x}}, \quad (24c)$$

where \mathbf{k}_h is the horizontal (i.e., tangential) co-moving wavenumber vector. The perturbed Euler equation (20) reads, component by component,

$$\rho \frac{d^2}{dt^2} \begin{bmatrix} \xi \\ \boldsymbol{\xi}_h \end{bmatrix} + 2 \frac{\dot{a}}{a} \rho \frac{d}{dt} \begin{bmatrix} \xi \\ \boldsymbol{\xi}_h \end{bmatrix} + \frac{1}{a} \begin{bmatrix} \partial \Delta P / \partial r \\ i \mathbf{k}_h \Delta P \end{bmatrix} + \frac{\rho \tilde{\mathbf{g}}}{a} \begin{bmatrix} \partial \xi / \partial r \\ i \mathbf{k}_h \xi \end{bmatrix} = 0, \quad (25)$$

where $\tilde{\mathbf{g}}$ is defined by Equation (16). We also have the (approximated) condition of incompressibility

$$\frac{\partial \xi}{\partial r} + i \mathbf{k}_h \cdot \boldsymbol{\xi}_h = 0. \quad (26)$$

Dotting the horizontal component of the Euler equation by \mathbf{k}_h and eliminating from there $\boldsymbol{\xi}_h \cdot \mathbf{k}_h$ via the incompressibility condition, we retrieve

$$\Delta P = -\rho \left\{ \tilde{g} \xi + \frac{a}{k_h^2} \left[\frac{d^2}{dt^2} \frac{\partial \xi}{\partial r} + 2 \frac{\dot{a}}{a} \frac{d}{dt} \frac{\partial \xi}{\partial r} \right] \right\}. \quad (27)$$

Inserting this into the radial component, after some algebra we find

$$\rho k_h^2 \left[\frac{d^2 \xi}{dt^2} + 2 \frac{\dot{a}}{a} \frac{d \xi}{dt} \right] - \frac{\partial}{\partial r} \left[\rho \left(\frac{d^2}{dt^2} \frac{\partial \xi}{\partial r} + 2 \frac{\dot{a}}{a} \frac{d}{dt} \frac{\partial \xi}{\partial r} \right) \right] - (\rho_a - \rho_b) \delta(r - R) \frac{\tilde{g} k_h^2}{a} \xi = 0, \quad (28)$$

where we have neglected the spatial variation of the effective gravity \tilde{g} on the scales we are concerned with; the delta term stems from the radial derivative of the unperturbed discontinuous density profile (12).

We further simplify the RTI criterion given by Equation (28). In our frame of reference the background is static, so $d/dt = \partial/\partial t$. Equation (28) must be solved separately inside and outside the bubble, i.e. for $r \gtrless R$. The two branches are not independent of each other, but are linked by the jump condition imposed by the delta function in Equation (28). For $r \neq R$ Equation (28) reduces to

$$k_h^2 \left(\partial_{tt}^2 \xi + 2 \frac{\dot{a}}{a} \partial_t \xi \right) - \left(\partial_{tt}^2 \partial_{rr}^2 \xi + 2 \frac{\dot{a}}{a} \partial_t \partial_{rr}^2 \xi \right) = 0. \quad (29)$$

For this equation we look for solutions in the separate form

$$\xi(r, t) = \phi(t) \zeta(r). \quad (30)$$

We find

$$\frac{d^2 \zeta}{dr^2} - k_h^2 \zeta = 0, \quad (31)$$

so Equation (29) has the piecewise solution

$$\xi(r, t) = \begin{cases} \phi(t) e^{-k_h (r-R)} & r > R \\ \phi(t) e^{k_h (r-R)} & r < R. \end{cases} \quad (32)$$

The function $\phi(t)$ is determined by the jump condition across the surface of discontinuity $r = R$. We integrate Equation (28)

over the thin layer $[R - \epsilon, R + \epsilon]$, where $\epsilon \rightarrow 0$. After some algebra we derive

$$\lim_{\epsilon \rightarrow 0} \left[\rho_0 \left(\frac{d^2}{dt^2} \frac{\partial \xi}{\partial r} + 2 \frac{\dot{a}}{a} \frac{d}{dt} \frac{\partial \xi}{\partial r} \right) \right]_{R-\epsilon}^{R+\epsilon} = -\frac{\tilde{g}(R) k_h^2}{a} \phi(t) (\rho_a - \rho_b), \quad (33)$$

where on the right-hand side we have used the identity $\phi(t) = \xi(r = R, t)$.

We now may insert the solution (32) into the jump condition (33) to get our equation for the evolution of the Lagrangian perturbation:

$$\frac{d^2 \phi}{dt^2} + 2 \frac{\dot{a}}{a} \frac{d\phi}{dt} - \frac{\tilde{g} k_h}{a} \frac{\rho_a - \rho_b}{\rho_a + \rho_b} \phi = 0, \quad (34)$$

where the effective acceleration \tilde{g} must be evaluated on the top of the bubble.

Note that if $a = \text{constant}$ this formula would reduce to the familiar RTI equation

$$\frac{d^2 \phi}{dt^2} = |g| k_h \frac{\rho_a - \rho_b}{\rho_a + \rho_b} \phi, \quad (35)$$

the growing solution of which is the exponential $\phi \propto e^{n t}$, with

$$n^2 = |g| k_h \frac{\rho_a - \rho_b}{\rho_a + \rho_b}. \quad (36)$$

If $\rho_a > \rho_b$, i.e. the denser fluid lies on top of the lighter one, then $n^2 > 0$: the perturbations grows exponentially as in the standard scenario of the RTI.

In the case of the inflating bubble, it is convenient to express the coefficients of Equation (34) terms of physical (rather than co-moving) variables. The effective gravity on the top of the bubble is

$$\tilde{g} = |g(r_b + R_b)| + \ddot{R}_b(t), \quad (37)$$

The wavelength $\lambda_h = 2\pi/k_h$ in all our equations is a *co-moving* quantity, so its magnitude does not have a precise meaning *per se*, but only when it forms a dimensionless quantity with the curvature radius R_b of the bubble. The dimensionless quantity

$$\varkappa = k_h(t) R_b(t), \quad (38)$$

i.e. the ratio between the bubble circumference and the perturbation's *physical* wavelength is frozen in time, since the perturbation is stretched by the expansion of the bubble. In the last equation we have written $k_h(t)$ to remark that here this wave number refers to a wave in physical (i.e. non-comoving) coordinates. In order to be consistent with our planar approximation, the factor \varkappa must be large. Finally, since the bubble's density is always much lower than the ambient density

$$\rho_b \ll \rho_a, \quad (39)$$

we write down the final expression of the perturbation equation in the form

$$\frac{d^2 \phi}{dt^2} + \frac{6}{5} \frac{1}{t} \frac{d\phi}{dt} - \varkappa \frac{|g| + \ddot{R}_b(t)}{R_b(t)} \phi = 0, \quad (40)$$

where we used Equation (6) to substitute for \dot{a}/a . It is worth to remember that ϕ is a co-moving variable: its link with the "physical" amplitude $\phi_{\text{phys}}(t)$, i.e. the amplitude expressed in non-comoving coordinates is given by the relation

$$\phi(t) = \phi_{\text{phys}}(t)/R_b(t). \quad (41)$$

The qualitative properties of Equation (40) are briefly discussed in the next Subsection.

3.3 Properties of the Rayleigh–Taylor Instability of an Inflating Bubble

Equation (40) differs from the standard equation for the Rayleigh–Taylor instability in three respects.

(i) The term proportional to $d\phi/dt$. This is essentially due to the fact that the unperturbed bubble is inflating; this term is therefore akin to the "Hubble drag" in the equations for the evolution of cosmological perturbations in an expanding Universe (see e.g. Peacock 1999, page 470).

(ii) The total acceleration \tilde{g} is made up by two contributions, the gravitational acceleration and the inflation deceleration. We have already illustrated how this may affect the onset of the RTI (see the discussion of Equation (4) in § 2).

(iii) The last term in Equation (40) is proportional to R_b^{-1} . Again, this is an effect of the co-moving frame: the factor R_b^{-1} stems from the fact that on account of the stretching due to the inflation all the co-moving lengths are larger by a factor $\propto R_b(t)$ than their non-comoving counterparts.

It is also instructive to give some insight in the qualitative behaviour of the solution of Equation (40). The coefficients of Equation (40) are singular for $t \rightarrow 0$, which is expected because the inflation starts at $t = 0$. Since $\ddot{R}_b < 0$, at early stages the acceleration is dominated by inflation, and Equation (40) can be approximated by

$$\frac{d^2 \phi}{dt^2} + \frac{6}{5} \frac{1}{t} \frac{d\phi}{dt} + \frac{6}{25} \varkappa \frac{\phi}{t^2} \sim 0. \quad (42)$$

This equation admits analytical solution of the form $\phi \propto t^\eta$, where the complex index

$$\eta = -\frac{1}{10} \pm \frac{1}{10} \sqrt{1 - 24 \varkappa}. \quad (43)$$

is solution to the quadratic equation

$$\eta^2 + \frac{1}{5} \eta + \frac{6}{25} \varkappa = 0. \quad (44)$$

The wavenumber of a perturbation is clearly limited by the size of the bubble: since $\varkappa \geq 1$, the argument of the square root is always *negative*: rearranging the real and imaginary part of t^η ,

$$\phi(t) = (t/t_0)^{-1/10} \{A \cos[\omega \log(t/t_0)] + B \sin[\omega \log(t/t_0)],\} \quad (45)$$

where t_0 is an arbitrary time and

$$\omega = \frac{1}{10} |24 \varkappa - 1|^{1/2}. \quad (46)$$

Apart from the oscillating factor, the co-moving perturbation amplitude ϕ decays as $t^{-1/10}$, showing that the bubble is Rayleigh–Taylor *stable*. In non-moving coordinates (see Equation (41)) this the amplitude grows as $\phi_{\text{phys}} \propto t^{1/2}$, i.e. less than the bubble radius $R_b \propto t^{3/5}$. The acceleration is inflation-dominated, and is directed upwards: this and the relative stratification of the bubble and the overlying medium imply that the configuration is stable, as found. Note that the ‘‘Hubble drag’’ term in Equation (40) plays a fundamental role in this decay. Without this term the early-time equation (42) would read

$$\frac{d^2 \phi}{dt^2} + \frac{6}{25} \varkappa \frac{\phi}{t^2} \sim 0. \quad (47)$$

Again, this admits solutions in the form

$$\phi(t) = (t/t_0)^{1/2} \{A \cos[\omega' \log(t/t_0)] + B \sin[\omega' \log(t/t_0)],\} \quad (48)$$

with

$$\omega' = \frac{1}{10} |24 \varkappa - 25|^{1/2}. \quad (49)$$

In this case (apart from a slowly oscillating term) the amplitude *increases*, albeit at the somewhat slow pace $\phi \propto t^{1/2}$. This apparently strange result is correct, since the energy of the oscillations diminishes, as the following argument shows. Equation (47) is formally the equation of a harmonic oscillator with a time-dependent square angular frequency

$$\Omega^2 = \frac{6}{25} \frac{\varkappa}{t^2}. \quad (50)$$

It is well-known from analytical mechanics (see e.g. Arnold 1978) that the ratio

$$I = E/\Omega. \quad (51)$$

between the energy $E \sim \Omega^2 \phi^2$ of the oscillator and its angular frequency Ω is an adiabatic invariant. Therefore, since $\Omega \propto t^{-1}$, then $\phi \propto t^{1/2}$ and

$$E \propto t^{-1}, \quad (52)$$

which shows that the energy of the oscillations decreases.

4 NUMERICAL RESULTS

In this Section we solve numerically Equation (40), which describes the evolution of the co-moving Lagrangian amplitude ϕ (Equation (41)) of a Rayleigh–Taylor perturbation in a non-inertial frame of reference moving with the expansion of the bubble, given by Equation (3).

We refer our numerical calculations to the cluster A 2052: for the ambient density profile we adopt the β -model

$$\rho(r) = \frac{\rho_c}{[1 + (r/r_c)^2]^{3\beta/2}} \quad (53)$$

with $\rho_c = 5.7 \times 10^{-26}$ g cm⁻³, $r_c = 36.4$ kpc and $\beta = 0.56$, which provides an approximate fit to the deprojected density profile given by Blanton et al. (2001).

For the gravitational acceleration we assume the Navarro et al. (1997) profile calculated by Zakamska and Narayan (2003) on the same data by Blanton et al. (2001):

$$g(r) = 2 g_0 (r/r_s)^{-2} \left[\log(1 + r/r_s) - \frac{r/r_s}{1 + r/r_s} \right] \quad (54)$$

where $r_s = 340$ kpc and $g_0 = 2.8 \times 10^{-8}$ cm s⁻².

The radius of the bubble (see also Equation (3) and Soker et al. 2002) is

$$R_b(t) = 7.8 \text{ kpc} \left(\frac{\dot{E}}{10^{44} \text{ erg s}^{-1}} \right)^{1/5} \left(\frac{t}{10^7 \text{ yr}} \right)^{3/5} \left(\frac{\rho_a}{10^{-25} \text{ g cm}^{-3}} \right)^{-1/5}. \quad (55)$$

In our calculation we must also take into account the buoyancy of the bubble: the drag force limits the bubble rise velocity to the uniform terminal velocity ¹

$$v_b^2 = \frac{8}{3} \frac{|g| R_b(t)}{C_D} \quad (56)$$

where (following Churazov et al. 2001) we set the drag coefficient $C_D \sim 0.75$. This velocity is slow enough to allow us to simply update at every integration step the values of $|g|$ and ρ_a with the values of the new environment in which the bubble is embedded.

The choice of the initial integration time t_0 and of the initial condition are not fully trivial, on account of the singularity of the equation for $t = 0$. We choose an “early” value of t_0 , meaning that at this time the inflation acceleration \ddot{R}_b is still dominant over gravity. At this time we fix the value of ϕ , the ratio between the physical (i.e., non-co-moving) amplitude of the perturbation and the radius of the bubble (see Equation (41)):

$$\phi(t = t_0) = \phi_0. \quad (57a)$$

Differentiating Equation (41) we get

$$\dot{\phi}(t = t_0) = \dot{\phi}_0 = \phi_0 \left(\frac{1}{t_p} - \frac{3}{5} \frac{1}{t_0} \right); \quad (57b)$$

the derivative $\dot{\phi}$ measures the relative magnitude of the growth time scales of the perturbation $t_p = \phi_{\text{phys}}/\dot{\phi}_{\text{phys}}$ and $t_b = R_b/\dot{R}_b = 5t_0/3$ of the bubble. We have integrated numerically Equation (40), with a fifth-order adaptive Runge–Kutta numerical algorithm (Press et al. 1992). We have explored its solutions for different values of the initial conditions (57). We have stopped (quite arbitrarily) the integration at $t_{\text{max}} = 10^8$ yr after the inflation starts. This time is few times larger than the life times of the radio bubbles estimated by Bîrzan et al. (2004). Of course, we have ascertained that our result do not depend on our choice of t_{max} .

5 DISCUSSION OF THE NUMERICAL RESULTS

In Figure 1 we plot the evolution of R_b , \dot{R}_b and \ddot{R}_b for the specific case of a bubble released at $r_c = 5$ kpc from the cluster centre. In Figures 2, 3, 4, 5, 6 and 7 we plot the evolution of the co-moving amplitude $\phi(t)$ for different parameters:

- the initial perturbation amplitude ϕ_0 (see Equation (57a));
- the ratio between the growth time t_p of the perturbation and of the bubble t_b (see Equation (57b));
- the initial time t_0 at which the integration starts
- the distance r_c from the cluster centre at which the bubble is initially inflated;
- the factor $\varkappa = k_h R_b$, i.e. the ratio between the circumference of the bubble and the horizontal wavelength of the physical RT perturbation.

Finally, in Figure 8 we have plotted the modulus of the relative velocity of the RT perturbation with respect to the expanding front of the bubble. In all our calculations we have kept fixed the value of the energy injection rate $\dot{E} = 10^{44} \text{ erg s}^{-1}$.

In Figure (2) we show the effect of the different terms in Equation (40). The dashed line plots the modulus $|\phi|$ of the solution of Equation (40) in which the effects of the inflationary deceleration are neglected:

$$\frac{d^2 \phi}{dt^2} - \varkappa \frac{|g|}{R_b(t)} \phi = 0; \quad (58)$$

here inflation is only taken into account as a progressive growth of the bubble’s radius R_b . The dot–dashed line plots the solution of Equation (40) in which the inflationary deceleration is taken into account, but where the “Hubble drag” term (i.e., the term proportional to $\dot{\phi}$) is neglected:

$$\frac{d^2 \phi}{dt^2} - \varkappa \frac{|g| + \ddot{R}_b(t)}{R_b(t)} \phi = 0, \quad (59)$$

Finally, the solid line plots the solution of Equation (40) as it stands. The ICM density profile is given by Equation (53) and the gravity profile by Equation (54), and refer to the cluster A 2052.

In all cases the amplitude grows, leading to the eventual bubble disruption by the RTI. At the “equivalence time” $t_{\text{eq}} \sim 2 \times 10^7$ yr when the moduli of the gravitational acceleration and the inflation deceleration are equal, the amplitude

¹ This formula assumes that the interior of the bubble is much thinner than the surrounding environment.

$|\phi|$ is still small in the case described by Equation (40) (solid line), but is already well-developed in the case described by Equation (58) (dashed line) and in the case described by Equation (59) (dot-dashed line); in this latter case the perturbation oscillates, and on account of the adiabatic invariance of the ratio between the oscillations' energy and frequency, the amplitude increases as $\phi \propto t^{1/2}$ (see the discussion after Equation (47)). At t_{eq} the magnitude of $|\dot{R}_b|$ falls below the value of gravity, and the overall acceleration changes sign; the RTI sets in and after few t_{eq} the bubble is torn apart (but see also the next Section for more important details).

It may seem a little puzzling that the inclusion of the deceleration \ddot{R}_b may *shorten* the life time of the bubble. This behaviour depends on the magnitude of the quantity $n^2 = \varkappa |g|/R_b$, as we show with the following argument. If we ignore the time dependence of n^2 , then the solution of (58) grows exponentially:

$$\phi \propto e^{n t}. \quad (60)$$

On the other hand, Equation (59) at small times when inflation dominates has solution

$$\phi \propto t^{1/2}, \quad (61)$$

as discussed in § 3.3. In the extreme case $n^2 \gg 1$, then the solution (60) grows very fast, while the solution (61) is slower. At the opposite extreme $n^2 \ll 1$ the solution (60) keeps limited for $t \lesssim n^{-1}$, and is rapidly outgrown by the solution (61). Besides, from t_{eq} on, the oscillations in Equation (59) become unstable. By this time they have developed to a fairly large amplitude, which promptly blows up as soon as the instability sets in. Since the factor $n^2 = \varkappa |g|/R_b$ decreases with time on account of the bubble's inflation and uprising, the actual situation is close to the case $n^2 \ll 1$, which explains why the system with the bubble's deceleration included tends to live slightly less than the other.

The solid line plots the perturbation's evolution as described by the full equation (40). The amplitude oscillates, and initially decays as $\phi \propto t^{-1/10}$ on account of the ‘‘Hubble drag’’ (discussed after Equation (47)). After several equivalence times t_{eq} the Rayleigh–Taylor instability finally takes over and disrupts the bubble. Note that the effect of the Hubble drag is fundamental in lengthening the life time of a bubble. Incidentally, note that a very similar effect also occurs in the context of the evolution of cosmological perturbations; the Hubble expansion inhibits the perturbations, and in particular the density contrast grows as a mere power-law of time (e.g. Peacock 1999).

Figure 3 shows the results when the the initial perturbation is $\phi = 10^{-2}$. All other parameters as in Figure 2.

In Figure 4 the wavelength is one third that in Figure 2; all other parameters are the same. As expected, perturbation growth faster.

In Figure 5 the results of releasing the bubble at $r_c = 15$ kpc are presented. The bubbles lives a little longer. This will be discussed below.

Changing the initial condition of $\dot{\phi}$ does not change much the results, as is shown in Figure 6; all other parameters as in Figure 2.

Figure 7 shows the effect of starting the perturbation at $t = 10^6$ yr instead of $t = 10^3$ yr; all other parameters as in Figure 2.

Finally, in Figure 8 we plot the modulus of the relative velocity $v_\phi = R_b \dot{\phi}$ of the perturbation with respect to the bubble front; note that at early times the perturbation is oscillating: this is the over-stable regime for the three cases calculated in Figure 2, which includes bubble acceleration, with (solid line) or without (dot-dashed line) the drag term. When the bubble acceleration is considered without the drag term (dot-dashed line), the perturbations attain quite high velocities. In the inner regions of cooling flow clusters the sound speed is

$$c_s = 5.2 \times 10^7 \text{ cm s}^{-1} \left(\frac{kT}{\text{keV}} \right)^{1/2}, \quad (62)$$

and therefore the perturbations oscillate with Mach numbers of $\mathcal{M} \sim 0.1 - 0.2$. At such fast motion some dissipation, which is not included in our calculation, is expected. The dissipation will slow down the growth of the instability in the over-stable regime (the oscillatory phase), making the bubble more stable already when the drag term is not included (dot-dashed line in Figures 2 and 8).

From the Figures some robust trends emerge.

(i) *Life time.* The life time of the bubble is always significantly (up to an order of magnitude) longer when the initial inflationary phase is accounted for (Soker et al. 2002). For typical values used here, the bubbles are torn apart by the RTI after a time $\gtrsim 10^8$ yr, assuming that the jet is active for $\sim 3 \times 10^7 - 10^8$ yr (Bîrzan et al. 2004). This is enough to account for the existence of outer ghost bubbles in clusters of galaxies, whose ages are $\lesssim 10^8$ yr (Dunn et al. 2005).

(ii) *Bubble's location.* The bubble injected close to the cluster centre live shorter than those injected at larger distances. The reason is that the growth time of the RTI is proportional to $\lambda_h^{1/2}$ (Equation (1)). Bubbles near the centre expand at a lower rate (see Equation (3)), hence for a constant ratio $k_h R_b = 2\pi R_b / \lambda_h$ bubbles near the centre have shorter perturbation wavelength λ_h , and therefore the RTI evolves faster. Also, near the centre gravity is higher, also shortening the RTI growth time. Note that the effect of gravity is not very large in the Navarro et al. (1997) gravitational potential we have considered, but would be more relevant in presence of a steeper gravitational profile.

(iii) *Wavelength.* The instabilities with short wavelength (i.e. higher value of $\varkappa = k_h R_b$) develop first (see also Equation (1)). They may change somewhat the bubble boundary, but it is the large wavelength perturbations, $\lambda_h \sim R_b$ that will tear the bubble apart.

(iv) *Energy Injection Rate* We have run some calculations with a lower energy injection rate \dot{E} , without reporting the relative figures, since they are very similar to those already presented. As one might expect, a lower energy injection rate entails a weaker deceleration and a weaker drag, and hence a shorter bubble lifetime. For $\dot{E} = 10^{42}$ erg s⁻¹, for instance (i.e. two orders of magnitude less than the case presented in the paper), the equivalence time only halves: $t_{\text{eq}} \sim 10^7$ yr instead of $t_{\text{eq}} \sim 2 \times 10^7$ yr. The difference is not large, and is due to the weak dependence of the bubble radius on the energy injection rate ($R_b \propto \dot{E}^{1/5}$, see Equation (3)).

Before ending this Section, it is worth to compare our results with the numerical simulations of Brügggen et al. (2002), who studied numerically the evolution of radio bubbles during the active inflation phase. A detailed comparison is difficult, since Brügggen et al. (2002) include the effects of a possible Kelvin–Helmholtz instability (KHI), which we have neglected. The KHI resulting from the bubble shear velocity with respect to the outer environment shapes the bubble as a mushroom, especially for low energy powering AGN jets. The RTI, on the other hand, tends to disrupt the top of the bubble first. As it is apparent from Figures 2, 4 and 5 of Brügggen et al. (2002), the top of the bubble keeps its round shape even if the jet is weak, showing that the RTI is not very relevant at this stage. Also the dependence of the lifetime of a bubble on the \dot{E} supplied by the jet agrees qualitatively with our results, although a more quantitative assessment is difficult. We also note that the flow of the ICM along the bubble sides as the bubble rises, will stretch the magnetic field lines along the flow direction. This builds the right tension to suppress the KHI (De Young 2003). It is much more difficult to build a magnetic field to stabilise the top front against the RTI, however. Therefore, although we claim that magnetic fields are not required to protect the bubble against the RTI, we do accept that they can suppress the KHI.

6 THE POST-INFLATION PHASE

The results presented in the previous Sections refer to an early phase of the lifetime of a bubble, when it is still powered by the jet launched by the central AGN. It is important to stress that this is a crucial assumption for our model. Yet, the jet cannot power the expansion indefinitely, and after few 10^7 yr (e.g. Alexander and Leahy 1987; Bîrzan et al. 2004) the jet fades. At the end of this “active” inflation phase the amplitude of the perturbations has been slightly suppressed by the drag and deceleration effects (see Equation (45), or Figure 2), so the instabilities will take more time to develop fully. After the jet switches off, the bubble rises buoyantly due to its low density. The process is almost adiabatic (there are but negligible heat exchanges between the bubble and the environment), so the bubble’s expansion is far too slow to induce a deceleration or a drag force strong enough to hinder the growth of the RTI. The RTI sets in, leading to the eventual disruption of the bubble itself.

At this stage the evolution of the bubble is quite difficult to follow analytically, on account of a host of new dynamical effects which will be discussed below. We refer to the existing literature for the numerical simulations of the evolution of these buoyant bubble, no more powered by an active jet (we refer in particular to Brügggen and Kaiser 2001 and Reynolds et al. 2005: since they do not include magnetic fields in their simulations, their results are more directly comparable to the case analysed in the present work).

In this Section we address briefly the most relevant physical effects occurring in the buoyant phase, as well as their influence on the growth of the bubbles’ instabilities.

After the end of the inflation’s stabilising effect (or after few times t_{eq} , when the deceleration and the drag are too weak to be relevant) the RTI is free to evolve. As the perturbations’ amplitude attains the magnitude $\phi_{\text{phys}}/\lambda_h \sim 0.1 - 0.2$, i.e. $\phi \sim 0.5 - 1/\varkappa$ the RTI enters the non-linear regime. Ofer et al. (1992) have shown that if the RT perturbations are not exactly monochromatic (which is the case in a realistic situation) the coupling between modes of different wavelengths suppresses the fast-growing short-wavelength modes; the overall effect is to suppress the growth of the instabilities, resulting in a further delay in the bubble disruption.

During the non-linear evolution the relative velocity of the bubble with respect to the ambient ICM may significantly affect the dynamics, with potentially dominant contributions from the KHI. There is another reason why the KHI becomes important only at this stage: in the early inflation phase the density contrast between the bubble interior and the ambient gas is very large, and in this situation the KHI is suppressed (Kaiser et al. 2005). Later on, however, when the density contrast lowers, the KHI may become important enough to be the primary cause for the bubble disruption.

Some authors suggest that the KHI growth rate may be reduced or suppressed in this phase. Kaiser et al. (2005) and Reynolds et al. (2005) show that the transport phenomena (plasma viscosity and thermal conduction) are able to suppress the growth of the fastest Rayleigh–Taylor and Kelvin–Helmholtz modes. This result is particularly important in the context of the present paper, since in the absence of an ordered magnetic field parallel to the bubble surface neither viscosity nor thermal conduction are expected to be strongly suppressed.

In the different context of the stability of cold fronts against the KHI Churazov and Inogamov (2004) have shown that if the interface between the interior of the bubble and the ICM has a finite thickness, the fast short-wavelength KHI modes are suppressed. As mentioned before, we do not expect the magnetic field to suppress the RTI, but we do expect it is able to reduce the growth of the KHI modes.

To summarise, even in the buoyant phase the growth of the instabilities may be reduced by the occurrence of several effects. We repeat that we do not expect them to prevent the final disruption of the bubble. The bubble *will* be torn apart, but on time scales of few 10^8 yr, consistent with the estimated ages of the “ghost” bubbles observed in several cooling flow clusters. The final onset of the RTI, with consequent disruption of the bubble, is only delayed but not avoided, which is consistent with ghost bubbles showing RTI features. Soker et al. (2002) suggest that the protrusion in the northwest bubble of the Perseus cluster (Fabian et al. 2000, 2002) is a clear signature of the late onset of the Rayleigh–Taylor instability.

7 SUMMARY

To summarise, our main conclusion is that the life time for X-ray deficient bubbles in cluster of galaxies, and the development of RTI features in ghost bubbles can be explained from pure gas dynamical effects, and there is no need to assume the existence of stabilising magnetic field. This conclusion is robust, and is not affected by the several simplifying assumptions we have made. For typical parameters, inclusion of the bubble inflation phase increases the expected life of bubbles by a factor of 5 – 10.

ACKNOWLEDGEMENTS

It is a pleasure to thank Adi Nusser for his fruitful observations. We also thank an anonymous referee, whose suggestions and criticism helped us to improve this paper. This research was supported in part by the Asher foundation at the Technion.

References

- Alexander, P. and Leahy, J. P.: 1987, *MNRAS* **225**, 1
- Arnold, V. I.: 1978, *Mathematical methods of classical mechanics*, Springer Verlag, New York, NY
- Baker, L.: 1983, *Physics of Fluids* **26**, 950
- Birzan, L., Rafferty, D. A., McNamara, B. R., Wise, M. W., and Nulsen, P. E. J.: 2004, *ApJ* **607**, 800
- Blanton, E. L., Sarazin, C. L., McNamara, B. R., and Wise, M. W.: 2001, *ApJ* **558**, L15
- Brüggen, M. and Kaiser, C. R.: 2001, *MNRAS* **325**, 676
- Brüggen, M., Kaiser, C. R., Churazov, E., and Enßlin, T. A.: 2002, *MNRAS* **331**, 545
- Castor, J., McCray, R., and Weaver, R.: 1975, *ApJ* **200**, L107
- Churazov, E., Brüggen, M., Kaiser, C. R., Böhringer, H., and Forman, W.: 2001, *ApJ* **554**, 261
- Churazov, E. and Inogamov, N.: 2004, *MNRAS* **350**, L52
- De Young, D. S.: 2003, *MNRAS* **343**, 719
- Dokuchaev, V. I.: 2002, *A&A* **395**, 1023
- Dunn, R. J. H., Fabian, A. C., and Taylor, G. B.: 2005, *MNRAS* **364**, 1343
- Fabian, A. C., Celotti, A., Blundell, K. M., Kassim, N. E., and Perley, R. A.: 2002, *MNRAS* **331**, 369
- Fabian, A. C., Sanders, J. S., Ettori, S., Taylor, G. B., Allen, S. W., Crawford, C. S., Iwasawa, K., Johnstone, R. M., and Ogle, P. M.: 2000, *MNRAS* **318**, L65
- Heinz, S., Choi, Y.-Y., Reynolds, C. S., and Begelman, M. C.: 2002, *ApJ* **569**, L79
- Jones, T. W. and De Young, D. S.: 2005, *ApJ* **624**, 586
- Kaiser, C. R., Pavlovski, G., Pope, E. C. D., and Fangohr, H.: 2005, *MNRAS* **359**, 493
- Landau, L. D. and Lifshits, E. M.: 1987, *Fluid Mechanics*, Butterworth-Heinemann, 2nd edition
- Livescu, D.: 2004, *Physics of Fluids* **16**, 118
- Mazzotta, P., Kaastra, J. S., Paerels, F. B., Ferrigno, C., Colafrancesco, S., Mewe, R., and Forman, W. R.: 2002, *ApJ* **567**, L37
- McNamara, B. R., Nulsen, P. E. J., Wise, M. W., Rafferty, D. A., Carilli, C., Sarazin, C. L., and Blanton, E. L.: 2005, *Nature* **433**, 45
- McNamara, B. R., Wise, M., Nulsen, P. E. J., David, L. P., Sarazin, C. L., Bautz, M., Markevitch, M., Vikhlinin, A., Forman, W. R., Jones, C., and Harris, D. E.: 2000, *ApJ* **534**, L135
- McNamara, B. R., Wise, M. W., Nulsen, P. E. J., David, L. P., Carilli, C. L., Sarazin, C. L., O’Dea, C. P., Houck, J., Donahue, M., Baum, S., Voit, M., O’Connell, R. W., and Koekemoer, A.: 2001, *ApJ* **562**, L149
- Navarro, J. F., Frenk, C. S., and White, S. D. M.: 1997, *ApJ* **490**, 493
- Ofer, D., Shvarts, D., Zinamon, Z., and Orszag, S. A.: 1992, *Physics of Fluids B* **4**, 3549
- Peacock, J. A.: 1999, *Cosmological Physics*, Cambridge University Press, Cambridge, UK
- Press, W. H., Teukolsky, S. A., Vetterling, W. T., and Flannery, B. P.: 1992, *Numerical recipes in C. The art of scientific computing*, Cambridge: University Press, 2 edition
- Reynolds, C. S., McKernan, B., Fabian, A. C., Stone, J. M., and Vernaleo, J. C.: 2005, *MNRAS* **357**, 242
- Shapiro, S. L. and Teukolsky, S. A.: 1983, *Black holes, white dwarfs, and neutron stars: The physics of compact objects*, Wiley Interscience, New York
- Soker, N., Blanton, E. L., and Sarazin, C. L.: 2002, *ApJ* **573**, 533, (SBS)
- Sun, M., Jones, C., Murray, S. S., Allen, S. W., Fabian, A. C., and Edge, A. C.: 2003, *ApJ* **587**, 619
- Vrtilek, J. M., Grego, L., David, L. P., Ponman, T. J., Forman, W., Jones, C., and Harris, D. E.: 2002, *APS Meeting Abstracts* p. 17107
- Zakamska, N. L. and Narayan, R.: 2003, *ApJ* **582**, 162

This paper has been typeset from a \TeX / \LaTeX file prepared by the author.

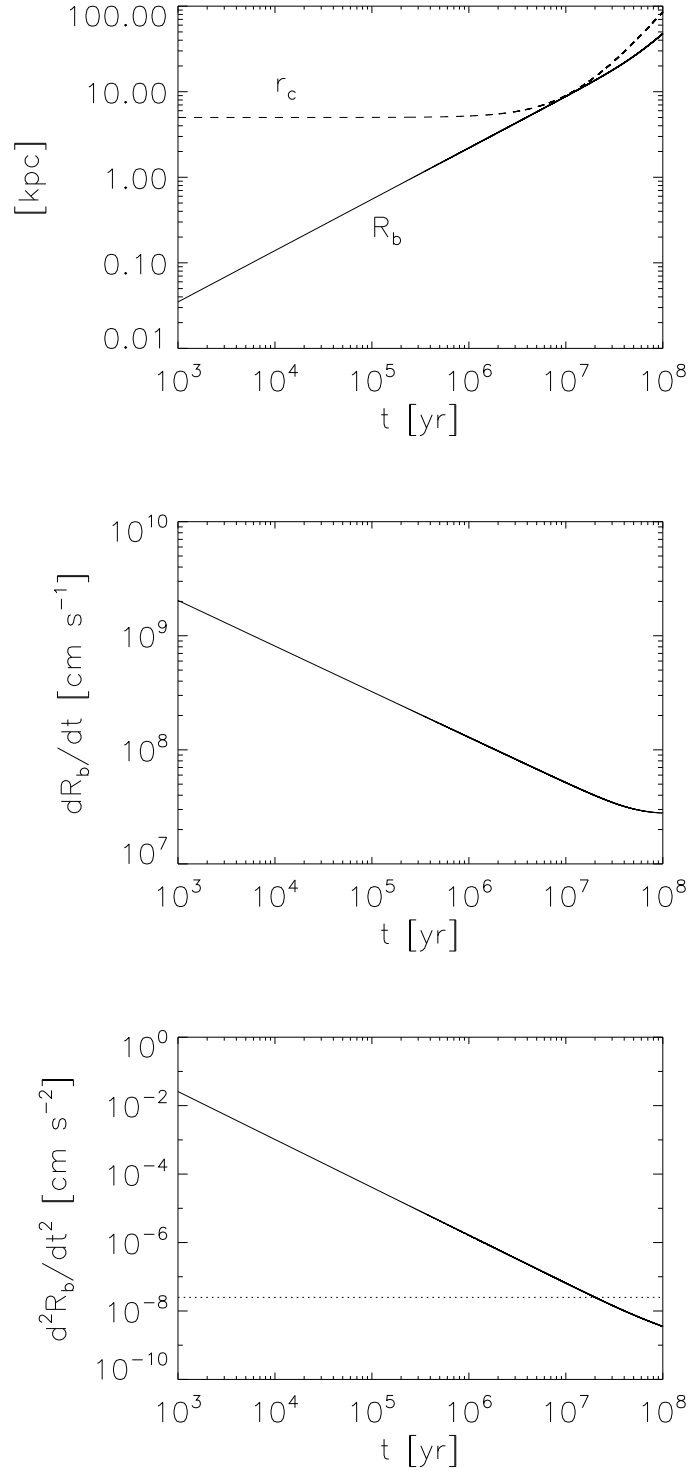


Figure 1. Upper panel: evolution of the radius of a bubble R_b (solid line) compared to the distance r_c between the centre of the bubble and the centre of the cluster (dashed line). Middle panel: expansion velocity \dot{R}_b of the bubble front. Lower panel: acceleration \ddot{R}_b of the bubble front. The dotted horizontal line shows the modulus $|g|$ of the gravitational acceleration at the position where it equals $|\dot{R}_b|$ on the top of the bubble. In this example the bubble is released at the initial distance $r_c = 5$ kpc from the centre.

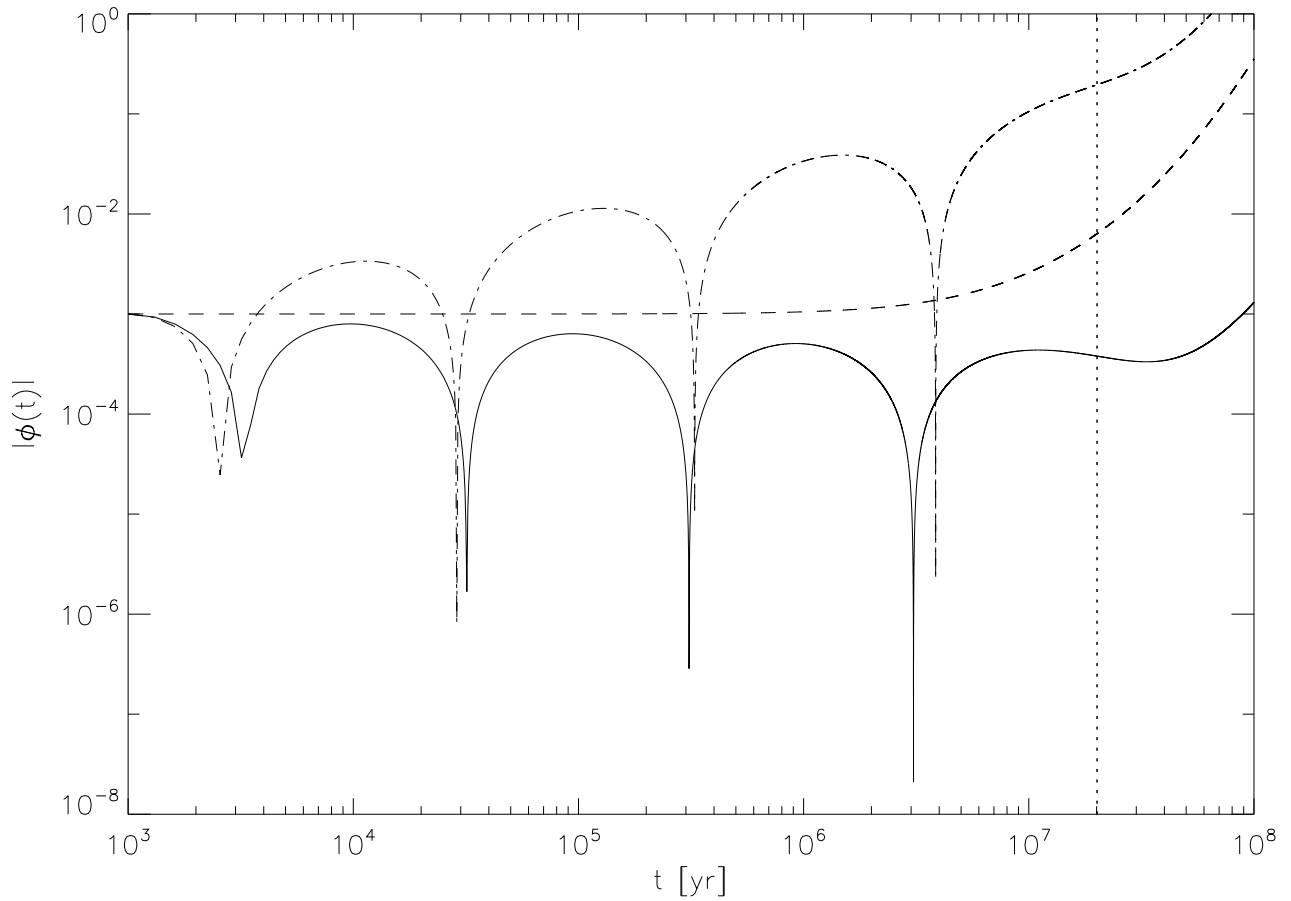


Figure 2. This plot compares the evolution the amplitude of a RTI of a perturbation in three cases. Plotted is the absolute value of the co-moving perturbation ϕ , i.e. the ratio between the real physical perturbation amplitude and the bubble’s radius R_b (Equation (41)). The cusps are artifacts of the logarithmic scale. In this example the bubble is released at $r_c = 5$ kpc from the centre, and the ratio between the circumference of the bubble and the wavelength of the physical perturbation is $\varkappa = 8$. The perturbation starts 10^3 yr after the bubble is born, with an initial co-moving amplitude $\phi_0 = 10^{-3}$ and zero relative velocity $\dot{\phi}_0 = 0$. The dashed line plots the case in which the inflation’s deceleration is neglected (Equation (58)). The dot-dashed line plots the evolution of the perturbation without the “Hubble drag” (Equation (59)). The solid line is the evolution described by the full equation (40). The dotted vertical line marks the time $t_{\text{eq}} \sim 2 \times 10^7$ yr when the acceleration \ddot{R}_b of the bubble front equals in magnitude the gravitational acceleration on the top of the bubble: $|\ddot{R}_b| = |g(r_c + R_c)|$. After 10^8 yr the RT perturbation is well developed in the cases described by Equations (58) and (59), but it is still small in the case described by Equation (40).

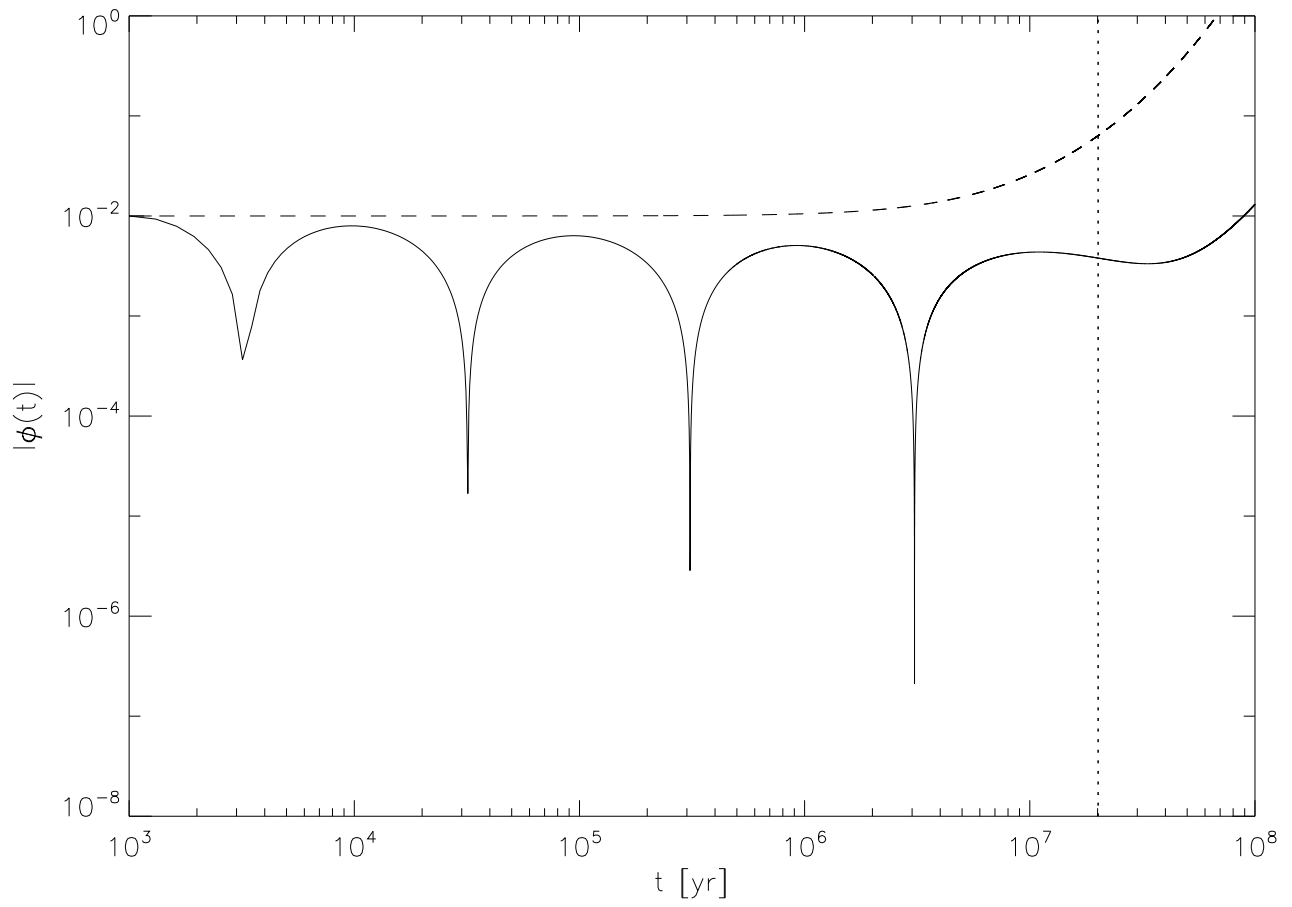


Figure 3. The lines have the same meanings as in Figure 2; also the parameters are the same, except the the initial relative amplitude, which here is $\phi_0 = 10^{-2}$.

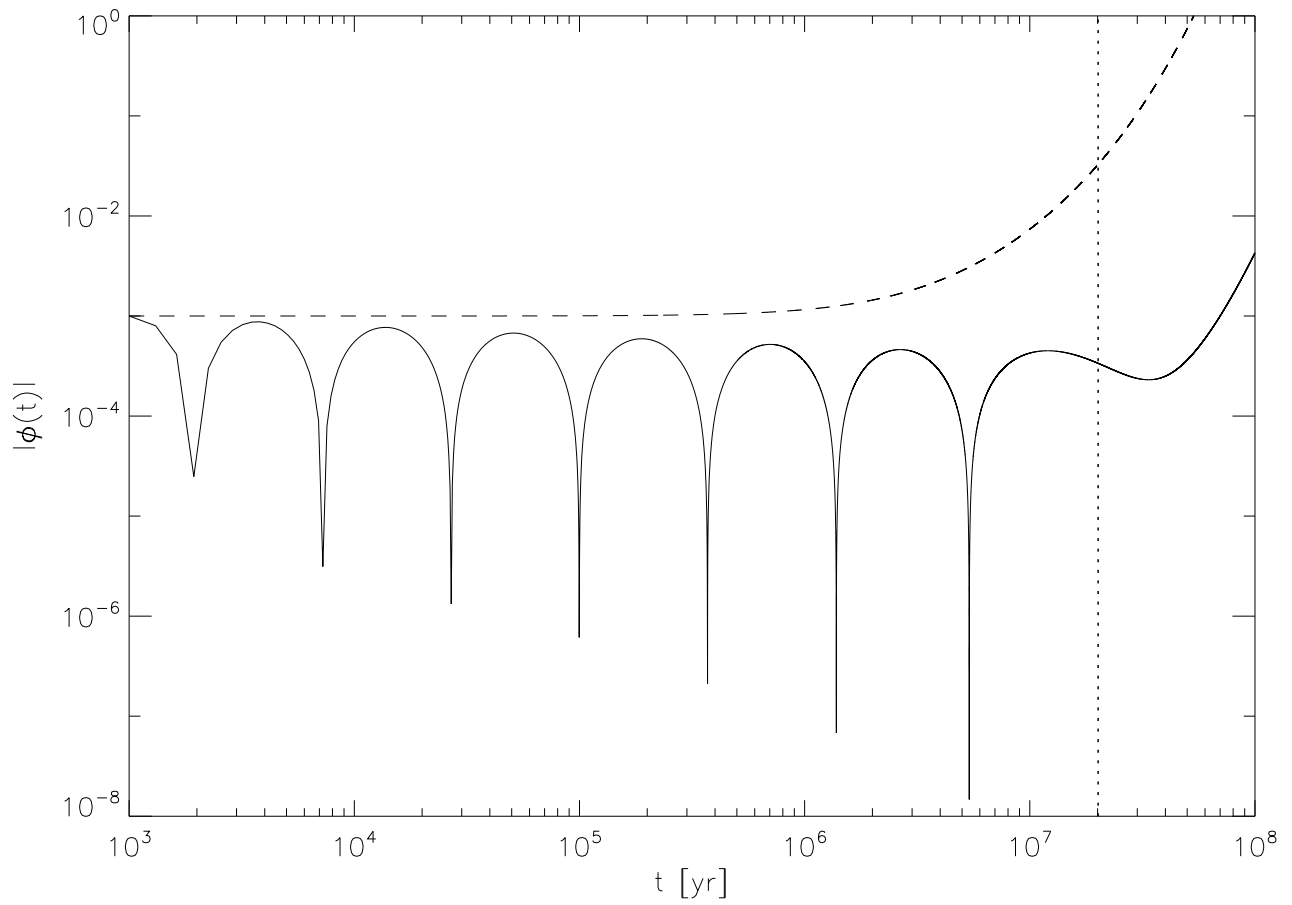


Figure 4. The lines have the same meanings as in Figure 2; also the parameters are the same, except the factor $\varkappa = k_h R_b = 24$. The short wavelength perturbations grow faster (see Equation (1)), although they are not responsible for the final RT disruption of the bubble.

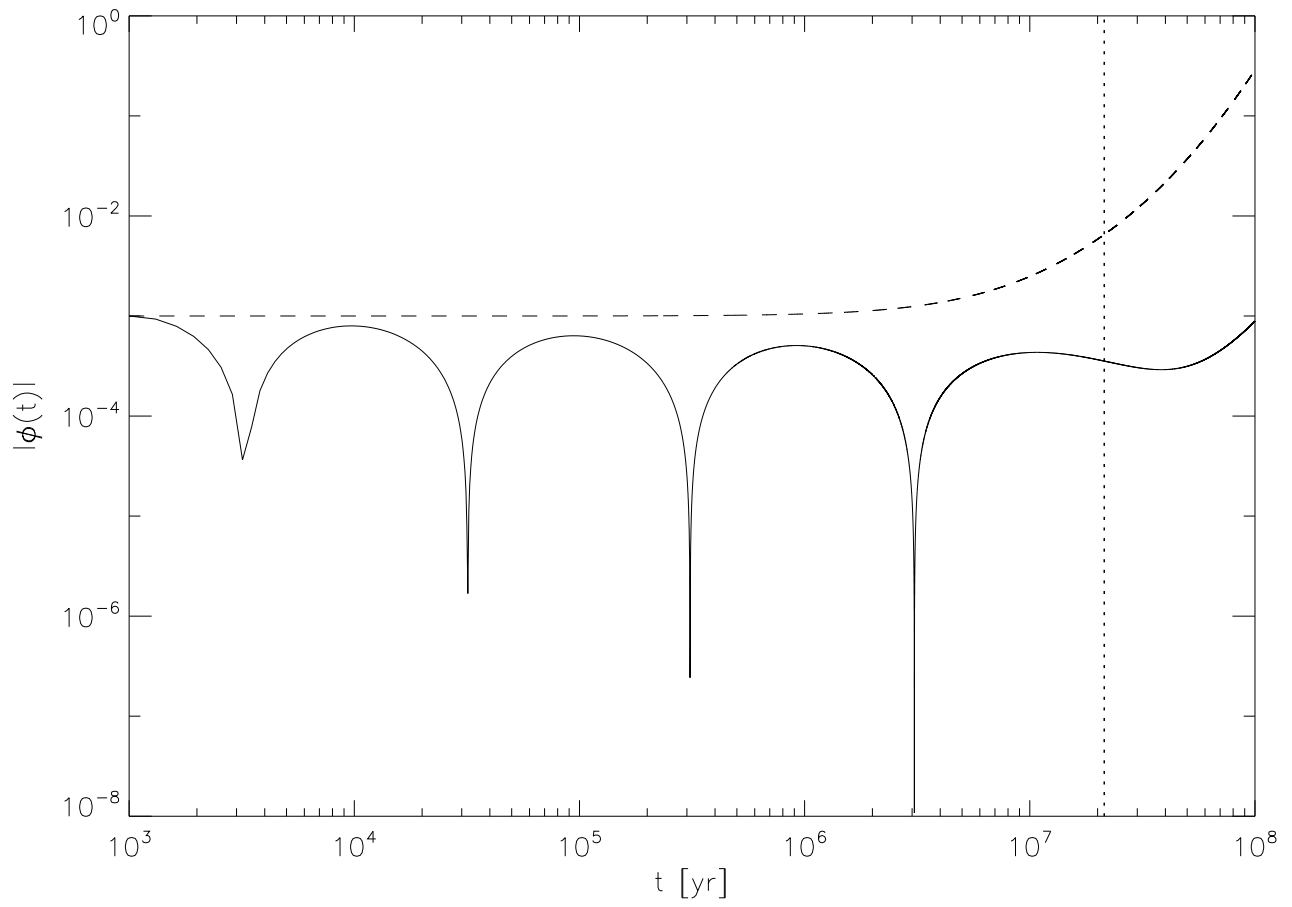


Figure 5. The same as in Figure 2, but with release radius $r_c = 15$ kpc.

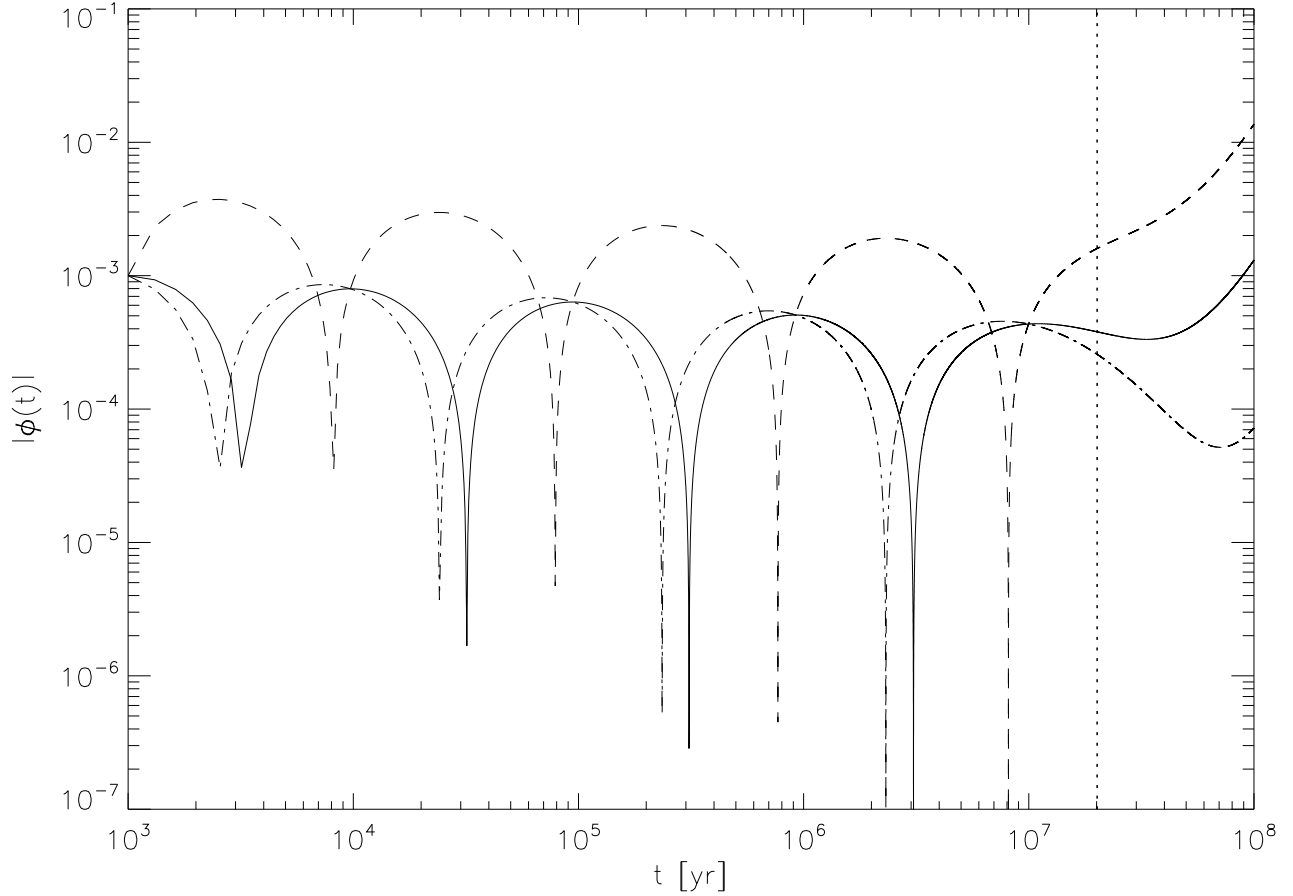


Figure 6. In this graph we show the effect of different initial velocities on the perturbation’s amplitude evolution, as described by Equation (40). The bubble is released at $r_c = 5$ kpc from the centre. The integration starts 10^3 yr after the inflation starts, with a parameter $\varkappa = 8$ and an initial relative amplitude $\phi_0 = 10^{-3}$. The dashed line corresponds to the initial condition (57b) with $t_p = t_b/10$, the solid line to $t_p = t_b$, and the dotted–dashed line to $t_p = 10 t_b$. As expected, the initially fastest–growing perturbations develop first, although the effect is not very large. The perturbations reach the amplitude $|\phi| = 0.5$ (at which we may consider the bubble as disrupted by the instability) at the times $t \sim 3.3 \times 10^8$ yr (case $t_p = t_b/10$), $t \sim 6.8 \times 10^8$ yr (case $t_p = t_b$), $t \sim 1.8 \times 10^9$ yr (case $t_p = 10 t_b$); there is a factor ~ 6 difference, while the ratio t_p/t_b spans two orders of magnitude. In all cases, the perturbation develops less than in the case without inflation (compare with Figure 2).

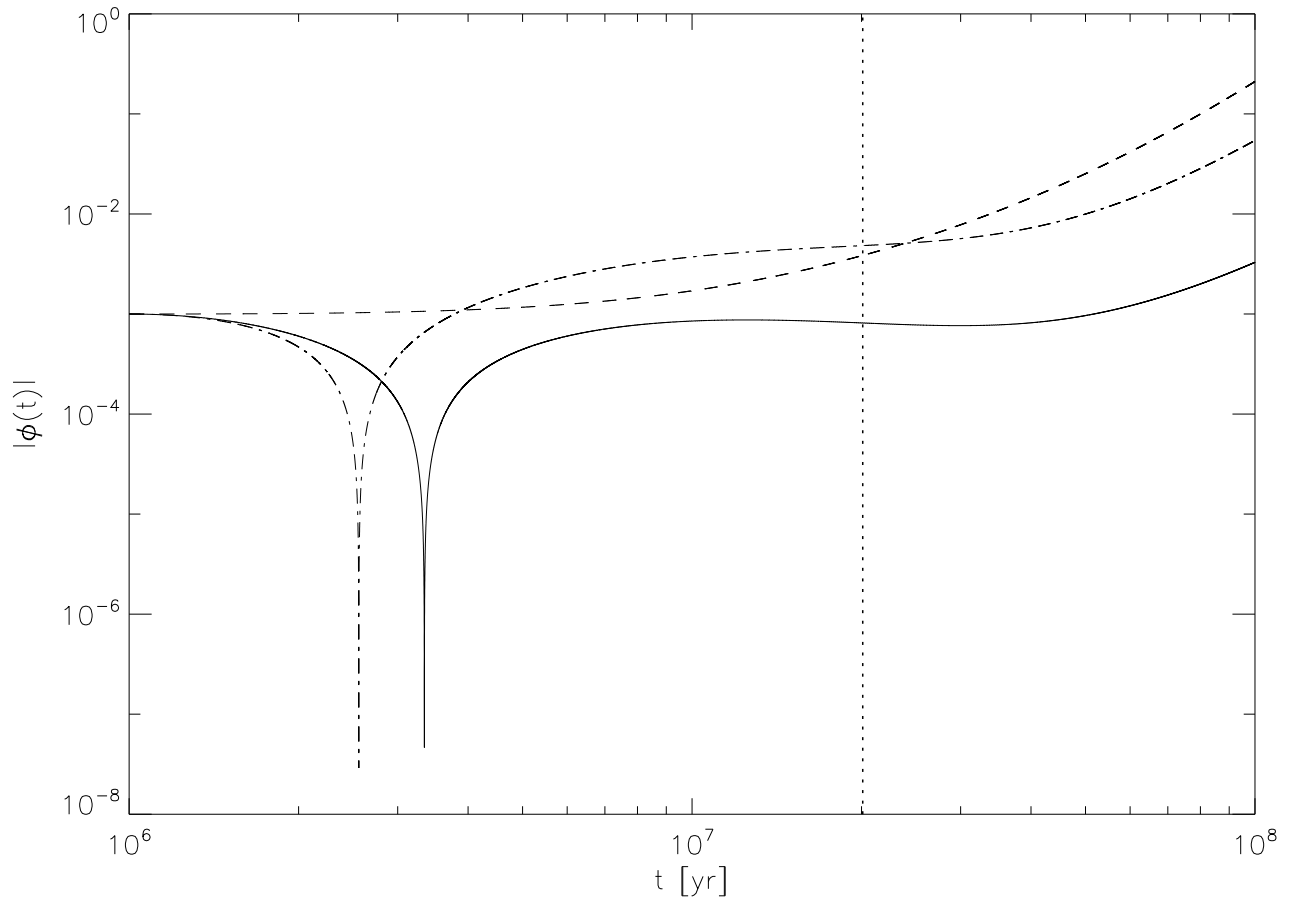


Figure 7. In this graph we show the effect of the choice of the initial integration time on the perturbation's amplitude evolution, as described by Equation (40). The parameters and the meaning of the lines are the same as in Figure 2, but the integration starts $t_0 = 10^6$ yr after the inflation onset. The difference between the case without acceleration (dashed line, Equation (58)), and the case without the Hubble drag (dot-dashed line, Equation (59)) is smaller. In the case without acceleration the repulsive force $\propto |g|/R_b(t)$ is smaller, since R_b starts from a larger value. In the case without the Hubble drag the oscillations do not have enough time to develop large enough amplitude before the time t_{eq} when they become unstable.

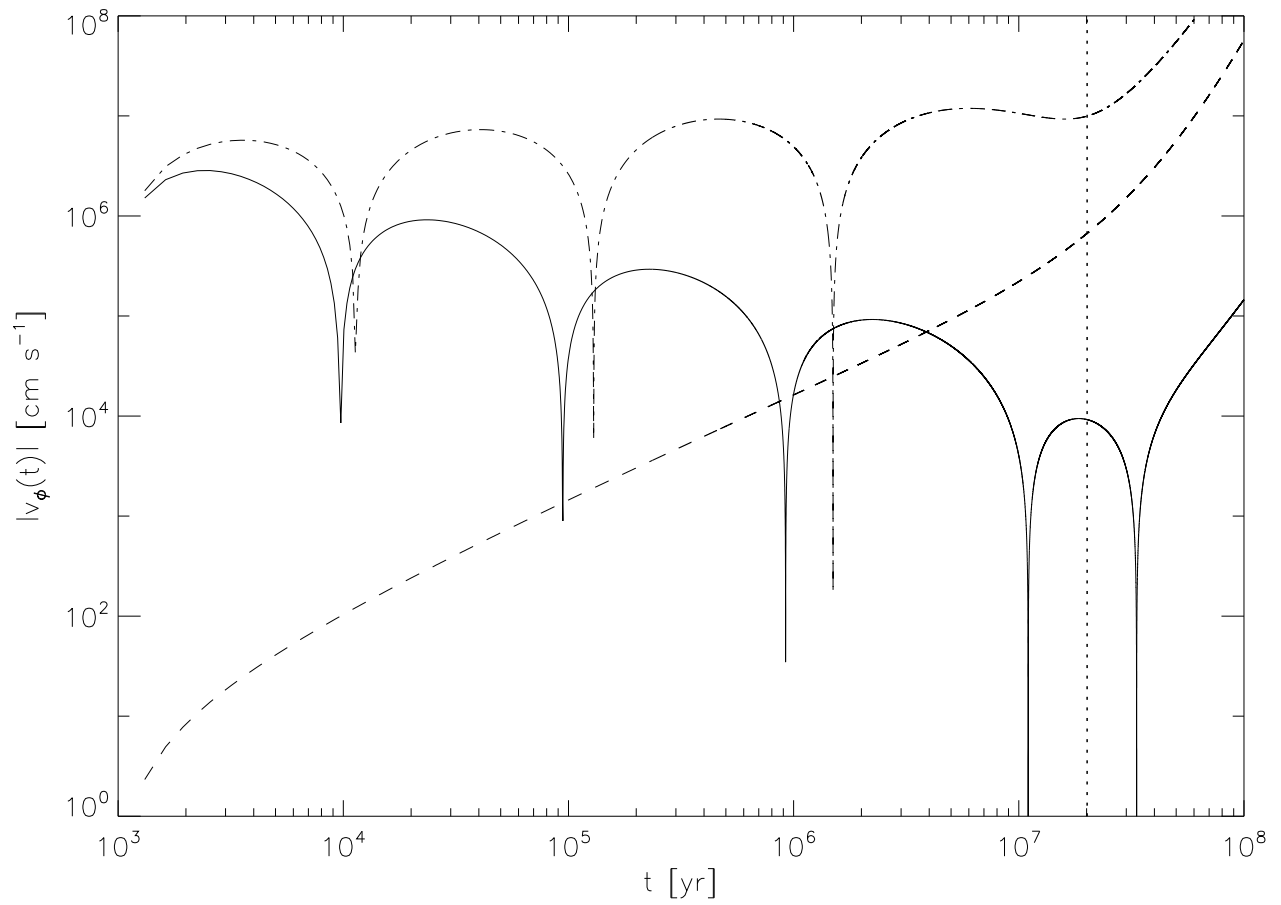


Figure 8. In this graph we show the modulus of the relative velocity $v_\phi = \dot{\phi} R_b$ of the perturbation with respect to the front of the expanding bubble. The parameters are the same as in Figure 2.